I&EC research
Industrial & Engineering Chemistry Research

Review

pubs.acs.org/IECR

# Thermodynamic Modeling with Equations of State: Present Challenges with Established Methods

Øivind Wilhelmsen,*[,†,‡] Ailo Aasen,[†,‡] Geir Skaugen,[‡] Peder Aursand,[‡] Anders Austegard,[‡] Eskil Aursand,[‡] Magnus Aa. Gjennestad,[‡] Halvor Lund,[‡] Gaute Linga,[‡] and Morten Hammer[‡]

[†]Department of Energy and Process Engineering, Norwegian University of Science and Technology, NO-7491 Trondheim, Norway
[‡]SINTEF Energy Research, NO-7465 Trondheim, Norway

**ABSTRACT:** Equations of state (EoS) are essential in the modeling of a wide range of industrial and natural processes. Desired qualities of EoS are accuracy, consistency, computational speed, robustness, and predictive ability outside of the domain where they have been fitted. In this work, we review present challenges associated with established models, and give suggestions on how to overcome them in the future. The most accurate EoS available, multiparameter EoS, have a second artificial Maxwell loop in the two-phase region that gives problems in phase-equilibrium calculations and excludes them from important applications such as treatment of interfacial phenomena with mass-based density functional theory. Suggestions are provided on how this can be improved. Cubic EoS are among the most computationally efficient EoS, but they often lack sufficient accuracy. We show that extended corresponding state EoS are capable of providing significantly more accurate single-phase predictions than cubic EoS with only a doubling of the computational time. In comparison, the computational time of multiparameter EoS can be orders of magnitude larger. For mixtures in the two-phase region, however, the accuracy of extended corresponding state EoS has a large potential for improvement. The molecular-based SAFT family of EoS is preferred when predictive ability is important, for example, for systems with strongly associating fluids or polymers where few experimental data are available. We discuss some of their benefits and present challenges. A discussion is presented on why predictive thermodynamic models for reactive mixtures such as $CO_2$−$NH_3$ and $CO_2$−$H_2O$−$H_2S$ must be developed in close combination with phase- and reaction equilibrium theory, regardless of the choice of EoS. After overcoming present challenges, a next-generation thermodynamic modeling framework holds the potential to improve the accuracy and predictive ability in a wide range of applications such as process optimization, computational fluid dynamics, treatment of interfacial phenomena, and processes with reactive mixtures.

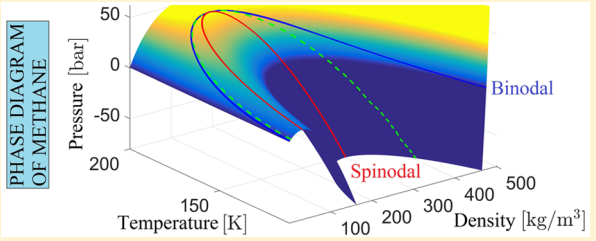


## INTRODUCTION

An accurate and robust thermodynamic framework is at the base of most higher-level modeling and simulation tools. Such a framework is central for handling problems of practical relevance such as two-phase flow of $CO_2$ mixtures[1] and design of heat exchangers[2−4] as well as problems of a more academic character, such as research on the thermal state of the earth's core[5] or discussions about water cavitation at highly negative pressures.[6] The typical framework has a collection of several equations of state (EoS), suitable for describing the properties of fluids or materials of interest, and algorithms to process the information in the EoS to provide the appropriate properties for a particular application. For instance, modeling of two-phase heat exchangers or distillation columns requires phase equilibrium calculations to be performed to obtain the relevant properties.

The accuracy of the thermodynamic model employed can have a large impact on higher-level modeling, and even on the final conclusions made in a study. For instance, the ice-like structures called hydrates can form and obstruct natural gas pipelines in the presence of even trace amounts of water. It is crucial for the petroleum industry to know the maximum allowable water content before hydrates can form to specify the appropriate dehydration requirements. However, the predicted maximum water content depends strongly on the choice of EoS.[7]

Hydrate formation is a good example of the type of challenges a modern state-of-the-art thermodynamic framework should be able to handle. The basis of hydrate equilibrium calculations with the van der Waals−Platteeuw model is an EoS capable of describing nonpolar, polar, and associating components.[8] The EoS should be easy to extend and improve when new experimental data are available to accommodate for new components and conditions. Moreover, the EoS should be thermodynamically consistent, incorporate known physical constraints, and be able to predict accurately outside of the domain where experimental data are available. Next, phase equilibrium calculations must be performed. Phase equilibrium calculations can be challenging and often time-consuming. In

**Received:** January 22, 2017
**Revised:** February 6, 2017
**Accepted:** March 10, 2017
**Published:** March 10, 2017

  

DOI: 10.1021/acs.iecr.7b00317
*Ind. Eng. Chem. Res.* 2017, 56, 3503−3515

hydrate equilibria, it is possible to have simultaneous coexistence of vapor, solid, and one or more liquid phases. It then becomes challenging to identify the thermodynamically most stable configuration.

It is generally accepted that no single EoS will be capable of describing all components or fluids, or be suitable for all applications.[9] In process simulations and time-consuming optimization studies, it is advantageous to use computationally efficient cubic EoS such as Peng–Robinson[10] or Soave–Redlich–Kwong.[11] When higher accuracy is needed, advantage is taken of corresponding state methods such as Lee–Kesler, extended corresponding state methods such as SPUNG,[12] or multiparameter EoS such as GERG-2008.[13−20] Models with enhanced predictive ability such as Statistical Associating Fluid Theory (SAFT) are preferred for certain applications, for example, for systems with strongly associating fluids or polymers where few experimental data are available.[21−23] It is clear that more work is needed to develop EoS for new fluids, especially polar and associating components such as electrolytes.[24] In this work, however, we shall discuss some of the fundamental challenges associated with the EoS and the basic routines found in current state-of-the-art thermodynamic modeling frameworks. Moreover, we shall discuss how to overcome these challenges. By overcoming them, a next-generation thermodynamic framework holds the potential to improve the accuracy and predictive ability in a wide range of applications such as process optimization, computational fluid dynamics, treatment of interfacial phenomena, and processes with reactive mixtures such as in distillation columns.

## STRUCTURE OF THE THERMODYNAMIC FRAMEWORK

From a programming point of view, a modern thermodynamic framework should be modular and easy to maintain and update. It is important to test the accuracy and robustness of EoS to ensure a thermodynamically consistent implementation. Automatic routines for consistency checks reduce the risk of programming errors and development of inconsistent EoS.[25] Moreover, it should be straightforward to add parameters for new EoS or new components. Postprocessing routines to plot phase envelopes and other thermodynamic data are natural parts of a modern thermodynamic framework. A natural structure of such a framework is illustrated in Figure 1, which represents a layer-type structure. Starting from the inner layer, the different layers can be described as follows:

**Database.** This is where the parameters for all available models and components in the framework are stored. This includes model constants, component-specific parameters for EoS models and ideal gas correlations, and interaction parameters for pairs of components for each model.

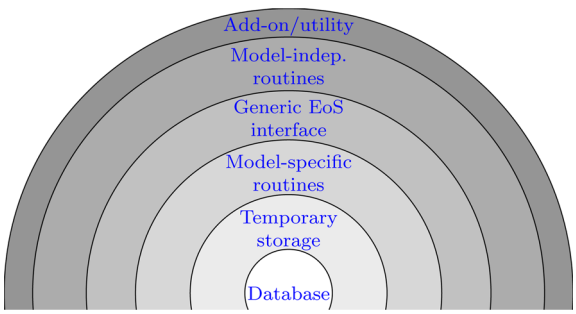


**Figure 1.** An illustration of the layer-based structure of a typical thermodynamic framework.

**Temporary Parameter Storage.** Since the database layer can grow large, it is more practical to work with a more compact structure for the components and the models currently selected, since only a small subset of the database is likely needed for a given application. This layer is structured to enable convenient writing of high performance property calculation routines.

**Model-Specific Routines.** These routines implement the specific thermodynamic models. On the basis of the temporary parameter storage, they calculate thermodynamic properties such as pressure, entropy, Gibbs energy, and their derivatives, using a specific model. These routines are mostly based on explicit analytical expressions, but it may also include model-optimized iterative routines such as density solvers.

**Generic EoS Interface.** These are wrapper routines around the model-specific routines. They simply redirect a property request to the appropriate routine from the currently chosen model. EoS-independent ideal gas contributions are then added in. This layer enables the writing of generic algorithms that can be ignorant about the underlying model.

**Model-Independent Routines.** These routines utilize the generic EoS interface to do calculations based on principles which are common to all consistent EoS. Examples include iteratively solving for bubble/dew points or multiphase equilibrium states, or checking for phase stability.

**Add-on and Utility Routines.** This layer includes, but is not limited to

- routines for result collection and plotting
- add-on models such as checking for possible formation of hydrates or other solids
- testing routines such as consistency checks
- framework for fitting model parameters to experimental data

A thermodynamic framework can be used as part of a process simulation or as part of a code to perform computational fluid dynamics (CFD). When accurate and computationally expensive thermodynamic models are needed, for example, in CFD dealing with compressible flows, thermodynamic calculations can become the bottleneck of the overall computation. It is therefore important that a modern thermodynamic framework lends itself easily to parallelization. Herein, one must consider both enabling simultaneous calls to serial routines in the library without causing memory collisions between separate instances and enabling routines in the library to utilize parallelization internally to solve its problem.

For the first point, a modular structure is needed with careful control of any shared memory. This can usually be achieved in a nonintrusive manner, with few implications to the actual core routines. For the second point, parallelizing routines require choosing algorithms that scale well in a parallel environment while minimizing overhead when run on a single processor. Here, shared memory approaches such as OpenMP offers flexibility, low code intrusiveness, and ease of implementation.

## MODELS IN THE THERMODYNAMIC FRAMEWORK

Desired qualities of thermodynamic models are accuracy, thermodynamic consistency, computational speed, robustness, and predictive ability outside the region with the data that has been used for fitting the model. The relative importance of these qualities depends on the application. Fiscal metering of


DOI: 10.1021/acs.iecr.7b00317
Ind. Eng. Chem. Res. 2017, 56, 3503−3515

$CO_2$ flow has extremely high accuracy demands, while computational speed and predictive ability are irrelevant. For integrated process optimizations in which the solvent used is also optimized, predictiveness is key since data are scarce for most solvents.[26] For large-scale CFD calculations where the uncertainties in the flow model dominate those in the thermodynamic model, and where flash calculations are called millions of times, computational speed and robustness take priority. Since no single thermodynamic model possesses all of these qualities, a flexible thermodynamic framework caters to these differing needs by implementing a range of thermodynamic models. The state-of-the-art modeling approaches within each of the areas are as follows:

**Accuracy/Consistency.** The most accurate thermodynamic models for predicting properties of gases and liquids are multiparameter EoS.[27,28] Although most consistency criteria are fulfilled, we shall highlight some important last hurdles multiparameter EoS must overcome.

**Computational Speed/Robustness.** At present, cubic EoS are preferred if high computational efficiency is needed. However, they can be inaccurate for predicting certain properties such as the density and the speed of sound in the liquid phase. We explore the possibility of enhancing the accuracy by exploiting the corresponding state concept, and also consider how this impacts computation time. For applications such as steady-state heat exchanger modeling, where the mixture composition is constant, another feasible approach is to tabulate the values from a high-accuracy EoS in a set of grid points (e.g., in the *TP*-plane) and then interpolate.[29]

**Predictive Capability.** For associating fluids and polymers with few available experimental data, it becomes necessary to employ EoS with enhanced predictive abilities such as SAFT and group contribution approaches. Moreover, to arrive at predictive thermodynamic models for mixtures such as $CO_2$−$NH_3$ and $CO_2$−$H_2O$−$H_2S$, EoS must be developed in close combination with phase- and reaction equilibrium theory. A predictive model must explicitly incorporate the underlying physical mechanisms such as chemical reactions and association. Qualitatively, ignoring association interactions in associating mixtures is similar to ignoring chemical reactions in reacting mixtures. Although one is often able to fit a simple cubic EoS to an associating (or reacting) binary system, models explicitly accounting for association (reactions) are needed to correctly predict the behavior of ternary or higher-order mixtures, due to cross effects such as several molecules associating (reacting) with the same molecule. We shall see that even for some *binary* mixtures, such as $NH_3$−$CO_2$, the performance of present EoS is very poor if reactions are neglected.

In the following, we discuss present research challenges associated with some of the main components of a modern thermodynamic framework: thermodynamic models and routines for calculating phase and reaction equilibria. In this discussion, we shall deal with challenges associated with each of the desired qualities elaborated above.

An overview of some common thermodynamic models and how they are connected is illustrated in Figure 2. The figure shows that there are many choices associated with cubic EoS, such as the type of alpha correlations, mixing rules, and incorporation of so-called volume shifts.[30] Further, the dashed lines elucidate that cubic EoS are used as input in many thermodynamic models such as corresponding state (CSP) models and the cubic plus association (CPA) EoS. Multiparameter EoS and Perturbed-Chain Statistical Associating Fluid Theory (PC-SAFT), however, do not rely on cubic EoS. Incorporating the association contribution in PC-SAFT and CPA involves choosing the number of association sites, as the figure shows.

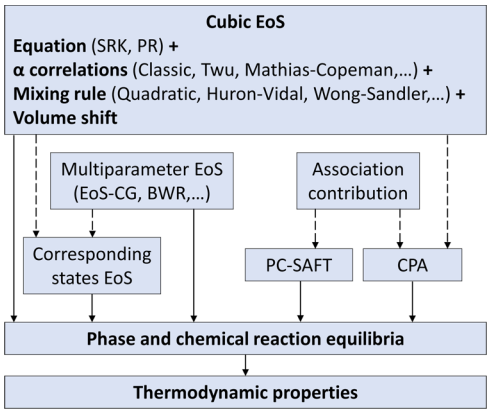


**Figure 2.** Overview of models. Dashed arrows represent submodels, and names in parentheses represent choices.

Finally we mention that an alternative to computing thermodynamic properties from EoS, is to use the so-called $\gamma-\phi$ approach: Here, the vapor phase is modeled with a conventional EoS (e.g., SRK), while an activity coefficient model is used for the liquid phase. These models will not be treated here due to their severe thermodynamic inconsistencies, for example, their inability to predict the existence of a vapor−liquid critical point.

## PRESENT CHALLENGES WITH ESTABLISHED METHODS

**Multiple Maxwell Loops in Multiparameter EoS.** The desire to represent the available experimental data in a compact and precise manner has motivated the development of state-of-the-art multiparameter EoS.[27] These equations are founded on a comprehensive analysis of experimental data and a diligent optimization procedure, with functional forms optimized for accuracy. Multiparameter EoS have been devised for single-component fluids[13−18] and mixtures.[20] The real fluid properties are in multiparameter EoS defined in terms of the following reduced Helmholtz energy function:[27]

$$\alpha_r(\delta, \tau) = \sum_k N_k \delta^{d_k} \tau^{t_k} + \sum_k N_k \delta^{d_k} \tau^{t_k} \exp(-\delta^{l_k}) + \sum_k N_k \delta^{d_k} \tau^{t_k} \exp\left(-\eta_k(\delta - \epsilon_k)^2 - \beta_k(\tau - \gamma_k)^2\right) \quad (1)$$

where $d_k$, $t_k$, $l_k$, $N_k$, $\epsilon_k$, $\gamma_k$, $\beta_k$, $\eta_k$ are fitted parameters, and $\delta$ and $\tau$ are the reduced density and the inverse reduced temperature. In addition, Gaussian terms with prefactors that diverge at the critical point, called nonanalytical terms, must be introduced to reproduce experimental data very close to the critical point.[27] Multiparameter EoS have unparalleled accuracy in the regions where thermodynamic data are available; however, they have challenges that restrict their popularity. For instance, they give substantially longer computational time than simpler EoS,[31] in particular for phase equilibrium calculations, where it is challenging to achieve robust and time-efficient calculations.[32]

The main reason for most of their current drawbacks is the second artificial Maxwell loop in the two-phase region.[27] Figure 3 demonstrates this using water at 550 K as example. Herein,


DOI: 10.1021/acs.iecr.7b00317
Ind. Eng. Chem. Res. 2017, 56, 3503−3515

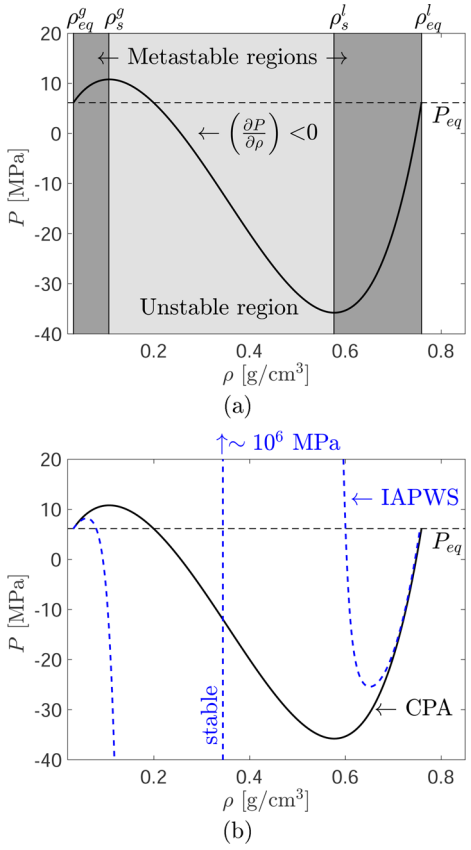


**Figure 3.** Pressure between the coexistence densities ($\rho^g_{eq}$ and $\rho^l_{eq}$) for water, as predicted by the CPA-EoS (solid lines)[33] in panels a and b and by the IAPWS-EoS (blue dashed line)[18] in panel b. The shaded regions in panel a illustrate where the single-phase fluid is metastable (dark shaded) and unstable (light shaded).

we have plotted the pressure, $P$, as a function of the density, $\rho$, within the two-phase region as predicted by the Cubic Plus Association (CPA) EoS (solid lines)[33,34] and the multiparameter IAPWS-EoS for water (blue dashed line).[18] "Maxwell loop", whose name is inspired by Maxwells equal area rule, denotes the behavior of the pressure as a function of the density, which displays a local maximum followed by a local minimum. While the CPA-EoS has only one Maxwell loop, the multiparameter EoS for water has two.

The second Maxwell loop gives a pseudostable homogeneous phase within the spinodals, $\rho^g_s$ and $\rho^l_s$, where subscript $s$ refers to the spinodals and superscripts g and l refer to gas and liquid, respectively. Moreover, the pseudostable phase has a lower Gibbs energy than the saturated fluid (vapor−liquid), thereby being the most stable phase. No experiments have ever shown a mechanically stable homogeneous phase within the spinodal states of water, where the single-phase fluid spontaneously decomposes into vapor and liquid since there is no longer any nucleation barrier to prevent phase change. Thus, the behavior of the IAPWS-EoS in the two-phase region represents an artifact of its functional form and parameters. Moreover, as shown by the blue arrow in Figure 3b, the value of the pressure diverges to $\pm 10^6$ MPa in the second, artificial Maxwell loop. As the magnitude of the peaks in the second loop exceeds the typical pressures at coexistence by orders of magnitude, numerical difficulties occur in phase-equilibrium calculations. The presence of the artificial second Maxwell loop and the problems it causes have for long been known to the experts developing multiparameter EoS.[27] We emphasize that such problems are also encountered with other EoS, such as modified Benedict−Webb−Rubin (mBWR) EoS.

With the goal of removing the second Maxwell loop of multiparameter EoS, Lemmon and Jacobsen modified in 2005 their functional form:[35]

$$\alpha_r(\delta, \tau) = \sum_k N_k \delta^{d_k} \tau^{t_k} + \sum_k N_k \delta^{d_k} \tau^{t_k} \exp(-\delta^{l_k}) + \sum_k N_k \delta^{d_k} \tau^{t_k} \exp(-\delta^{l_k}) \exp(-\tau^{m_k}) \quad (2)$$

where $m_k$ are additional fitted parameters. By adding terms consisting of a product of exponentials (third term on the right-hand side of eq 2), and using additional constraints in the nonlinear fitting routine, the authors managed to obtain a fit that gave smaller values of the parameters, $t_k$. This enabled Lemmon and Jacobsen to reduce the magnitude of the second Maxwell loop from $\sim 10^6$ MPa to below $\sim 10^2$ MPa. The behavior of the fluid they used as example, pentafluoroethane (known as R125) is shown in Figure 4a. The figure shows that

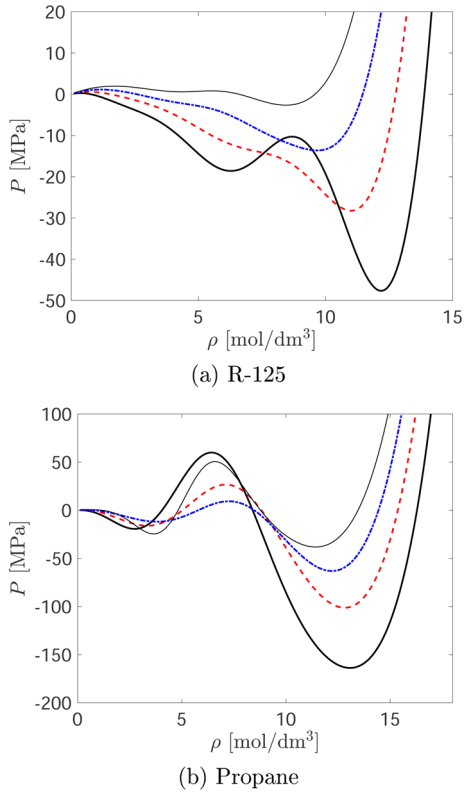


**Figure 4.** Pressure between the coexistence densities ($\rho^g_{eq}$ and $\rho^l_{eq}$) as predicted by the multiparameter EoS for R125[35] (a) at 180 K (black solid thick line), 220 K (red dashed line), 260 K (blue dash-dot line), and 300 K (black solid thin line), and as predicted by the multiparameter EoS for propane[28] (b) at 100 K (black solid thick line), 140 K (red dashed line), 180 K (blue dash-dot line), and 220 K (black solid thin line).

even if the second Maxwell root has a significantly smaller magnitude than in the case of water, the second loop is nonetheless still present. Lemmon and Jacobsen argued that for R125, the artificial second Maxwell loop was for all temperatures below the equilibrium pressure line. This was an


DOI: 10.1021/acs.iecr.7b00317
Ind. Eng. Chem. Res. 2017, 56, 3503−3515

important improvement compared to the behavior of previous multiparameter EoS, exemplified by Figure 3b.

The main progress in the work by Lemmon and Jacobsen toward removing the second artificial Maxwell loop was arguably in introducing new nonlinear constraints. Lemmon and Jacobsen implemented the constraint discussed by Elhassan et al.:[36]

$$a(\rho) - a_{\text{tang}}(\rho) \geq 0 \tag{3}$$

where $\rho$ is the density, $a$ is the Helmholtz energy and subscript "tang" means the Helmholtz energy evaluated at the equilibrium tangent line. Despite of what Elhassan and coauthors claim in their work,[36] the constraint in eq 3 does not "remove any inconsistencies between thermodynamic stability and physical reality". Even if eq 3 guarantees that both the Hemholtz energy and the Gibbs energy of the vapor−liquid coexistence state is lower than the corresponding energy state functions of a pseudostable state coming from a second Maxwell loop,[36] the pseudostable state can still be stable in other ensembles. For instance, in an isolated system where vapor and liquid coexist, the internal energy of the system should be lower than the internal energy of the pseudostable state. This does not follow from eq 3. Moreover, such constraints on the energy state functions do not exclude a second Maxwell loop with states that are **metastable** relative to the vapor−liquid coexistence. Such states are artifacts of the EoS, but may still appear as more stable than for example superheated vapor, supercooled liquid, or as a second liquid phase. They could thus artificially enter the phase diagram of single-component fluids and mixtures.

In 2009, Lemmon et al. presented a multiparameter EoS for propane, where they reverted back to the functional form with Gaussian bell shaped terms represented by eq 1.[28] By using the new fitting techniques and constraints from ref 35 they were able to reduce the values of the parameters $t_k$ and thus achieve a similar effect as the modified functional form in eq 2. They could thereby reduce the magnitude of the artificial Maxwell loop. Recent multiparameter EoS are formulated with the functional form in eq 1[37] and recent papers report that they use the new constraints presented in refs 28, 35, and 37.

The behavior of the multiparameter EoS for propane is shown in Figure 4b. The figure shows that the artificial second Maxwell loop is still present and has a larger magnitude than in the case of R-125 (Figure 4b). In contrast to the EoS for R-125, the second artificial Maxwell loop does not remain below the equilibrium pressure line. By examining the two-phase region of propane at 220 K (solid thin line in Figure 4b), we find that the solution with the lowest Gibbs energy at $P = P_{\text{eq}}$ is in fact the pseudostable state at a molar volume of $v \approx 0.2$ dm$^3$/mol, which stems from the second Maxwell loop. This means that the constraint in eq 3 is not satisfied for the EoS presented in ref 28, which is further confirmed by Figure 5.

Figure 5 plots the Helmholtz energy of the EoS (solid line) for propane at $T = 220$ K. The figure shows that the stable configuration as predicted from the EoS is a coexistence between the pseudostable state and liquid (blue dashed line) or vapor (blue dashed line), since these configurations have lower energies than the vapor−liquid coexistence (red dashed line). This is clearly unphysical, and it is an artifact of the multiparameter EoS and its parameters.

It is clear from the previous discussion that the second Maxwell loop in multiparameter EoS and the associated challenges have not yet been handled satisfactorily. In the next section, we shall discuss some of the benefits of a thermodynamic framework equipped with muliparameter EoS that have only one Maxwell loop in the two-phase region.

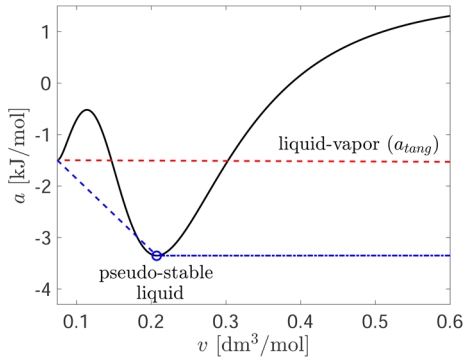


**Figure 5.** Helmholtz energy of the EoS (solid line), and the tangent line between vapor and liquid (red dashed line) for the multiparameter EoS for propane at 220 K.[28] The tangent line between the pseudostable state (circle) and liquid (blue dashed line) or vapor (blue dash−dot line). The figure shows that eq 3 is violated for propane at 220 K.

*Benefits of Consistent Multiparameter EoS.* There are several reasons for developing multiparameter EoS with a single Maxwell loop. To describe mixtures with multiparameter EoS, it is necessary to extrapolate to the metastable and unstable regions of the single-component fluids. A second artificial Maxwell loop will complicate the mixing rules of multiparameter EoS and introduce "unphysical" terms. Further, it makes phase equilibrium calculations with multiparameter EoS challenging and leads to a pseudostable state in the two-phase regime that is either stable or metastable with respect to the vapor−liquid coexistence. The pseudostable phase could appear in phase equilibria where several liquid phases are expected. In addition, the second artificial Maxwell loop excludes multiparameter EoS from important applications such as treatment of interfacial phenomena with mass-based density functional theory.

Figure 6 reports the time-average local density as a function of position through the interfacial region between vapor (left) and liquid (right). The solid line reports results from molecular dynamics (MD) simulations from ref 38, where particles interact through the truncated and shifted Lennard-Jones potential, giving properties similar to argon. As shown in the figure, densities in the metastable and unstable parts of Figure 3a occur locally across the interface region, where these states are stabilized by the steep density gradient. Interfacial phenomena can be studied using mass-based density functional theory, where the simplest variant is known as Square Gradient Theory (SGT). SGT obtains nonlocal thermodynamic properties by minimizing a constrained Helmholtz energy functional. The theory has been a key tool to investigate interfacial phenomena for more than 100 years, and was first introduced by van der Waals at the same time as he developed the van der Waals EoS which earned him the Nobel Prize in physics.[39] To obtain the density profile through the flat interface, one can solve the following second order differential equation which results from a minimization of a Helmoltz energy functional:[40]

$$\mu_{\text{eq}} = \mu_{\text{EoS}}(T, \rho(z)) - \beta \frac{\mathrm{d}^2\rho(z)}{\mathrm{d}z^2} \tag{4}$$



DOI: 10.1021/acs.iecr.7b00317
Ind. Eng. Chem. Res. 2017, 56, 3503−3515

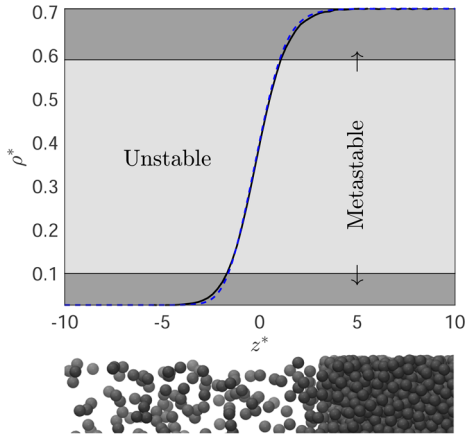


**Figure 6.** Time-average density profile from molecular dynamics simulations in reduced units (superscript *) through the vapor−liquid interface for the truncated and shifted Lennard-Jones fluid at a reduced temperature of 0.95 and truncation distance of 4 in reduced units (solid line), and results from SGT formulated as in ref 42 (blue dashed line). The bottom image shows an illustration of the particle density through the interface. The shaded regions illustrate where the single-phase fluid is metastable (dark shaded) and unstable (light shaded).

where $\mu_{eq}$ is the coexistence value of the chemical potential, $\mu_{EoS}$ is the value from the EoS, $T$ is the temperature, $\beta$ is a constant which can be determined from theory, and $z$ is the direction perpendicular to the interface. We have solved this model for the Lennard-Jones fluid using an accurate MBWR-EoS with a single Maxwell loop in the two-phase region,[41,42] and obtained the blue dashed line, which can hardly be distinguished from the time-average results from the MD simulations.

SGT relies on the thermodynamic properties of the homogeneous fluid in the metastable and unstable regions (see the shaded parts of Figures 3a and 6). Figure 6, and many other works,[38,42−44] show that SGT is then clearly capable of predicting interfacial properties to a high accuracy. Since multiparameter EoS have a second artificial Maxwell loop in the two-phase region, they cannot be used in this context. The reason is that the second Maxwell loop introduces a pseudostable homogeneous phase within the two-phase region, which contradicts the presence of a vapor−liquid interface. Thus, only EoS with a single Maxwell loop can give reasonable interfacial density-profiles with SGT.

Coupling of multiparameter EoS with SGT or more advanced density-functional theory to study interfacial properties can give extraordinary possibilities, not only in science, but also in industrial applications. SGT is commonly used to predict the surface tension, which is important to determine the flow pattern in multiphase pipeline flow.[45] Much of the deviation between experimental surface tensions and those predicted by SGT can be attributed to inaccuracies in the EoS.[46−48] Other important applications of SGT are to evaluate the leading order curvature corrections of the surface tension for correcting classical nucleation theory,[49] and to obtain the coefficients for describing heat and mass transfer across flat and curved interfaces.[38,50] The theory has provided insight into the interfacial properties of a wide range of systems such as solid hydrates,[51] crystals,[52] and biological systems.[53]

In summary, to remove the artificial second Maxwell loop from multiparameter EoS would enhance the accuracy of SGT and prediction of interfacial properties *in general*. In addition, it would to a large degree resolve the numerical challenges in phase-equilibrium calculations with multiparameter EoS, and reduce the computational time significantly due to a simpler density solver. In the next two subsections, we shall discuss how multiparameter EoS can be consistently extended to the metastable and unstable regions of the phase diagram of the single-phase fluid.

*Extending EoS to the Metastable Regions.* In Figure 3b, the regions, $\rho^g_{eq} < \rho < \rho^g_s$, and $\rho^l_s < \rho < \rho^l_{eq}$, define the metastable states of the single-phase fluid. Metastable states are ubiquitous in nature, for instance in water transported to the top of tall trees. Metastable states represent local minima in the energy landscape, but with higher energies than the coexistence between vapor and liquid. In laboratories, water has been supercooled down to an astounding 231 K at atmospheric pressure.[54] Metastable phases are now attracting more attention, and multiparameter EoS have been extended in this direction, for instance to describe supercooled water.[55] As the metastable fluid approaches the spinodal, the nucleation barrier becomes smaller and smaller, and the vapor will in practice transform into a saturated fluid long before $\rho^g_s$ has been reached due to thermal fluctuations that occur naturally at equilibrium. With present experimental techniques, one can only study the properties of the metastable fluid until the homogeneous nucleation limit has been reached. The single-phase fluid will then spontaneously decompose into vapor and liquid on a time scale which is too short to enable measurement of the fluid properties prior to nucleation.

A recent work shows how small, closed containers can be used to completely prevent nucleation, achieving infinitely long-lived metastable states, referred to as superstable.[56] Simple formulas were derived to predict accurately the conditions (container sizes) at which this superstabilization takes place. From a practical point of view, one is interested in the container radius, $R_{min}$, below which no nucleation can occur for a given initial supersaturation, $S = P^g_0/P_{eq}$, in formation of droplets, or a given initial external pressure (or stretching), $P^l_0$, in formation of bubbles, where subscript 0 denotes the initial state:

$$R^g_{min} \approx \frac{2\sigma}{\rho^l_{eq} k_B T \ln(S)} \left( \frac{\rho^l_{eq}}{\rho^g_{eq}} \left( \frac{\ln(S) + 7}{S \ln(S)} \right) \right)^{1/3} \quad (5)$$

$$R^l_{min} \approx \frac{2\sigma}{P_{eq} - P^l_0} \left( \frac{7}{\kappa^l_0 (P_{eq} - P^l_0)} \right)^{1/3} \quad (6)$$

where $\sigma$ is the surface tension, $k_B$ is Boltzmann's constant, and $\kappa$ is the compressibility. Equation 5 can be used in the region, $\rho^g_{eq} < \rho < \rho^g_s$, and eq 6 in the region $\rho^l_s < \rho < \rho^l_{eq}$. Equations 5 and 6 predicted the radius of a spherical container which makes the single-phase fluid superstable within an accuracy of 10%.[56]

Experiments and simulations that exploit superstabilization can be used to investigate the properties of highly metastable states in the future, in principle all the way to the spinodals. Experiments can be carried out in quartz inclusions, similar to those of ref 6, in which speed of sound measurements in the inclusion give information about the slope of $P(\rho)$ at constant entropy, similar to ref 57. Since such experiments are very challenging, the perhaps most available methodology to study the properties of highly metastable states is to use MD simulations in the canonical ensemble with volumes guided by


DOI: 10.1021/acs.iecr.7b00317
Ind. Eng. Chem. Res. 2017, 56, 3503−3515

eqs 5 and 6. For many fluids such as alkanes, carbon dioxide, and nitrogen, force fields have been developed that reproduce the thermodynamic properties from experiments very accurately.[58] Molecular Dynamics simulations are then capable of generating pseudoexperimental data in the metastable regions, or to possibly estimate the spinodals of the fluid. Another attractive possibility is to explore the potential of using quantum chemistry to predict key properties to a good accuracy by exploiting fundamental principles. For instance, Wheatley and Harvey[59] used quantum chemistry to obtain a model for the second cross virial coefficient for the $CO_2$−$H_2O$ system, and recently Meyer and Harvey[60] performed measurements that were consistent with the model predictions. Eventually, hybrid data sets with both experimental data and data from computations can be exploited in the fitting of the next generation multiparameter EoS, following a procedure similar to Rutkai et al.[61]

*Extending EoS to the Unstable Region.* There exists today no experimental technique that can stabilize a single-phase fluid in the unstable region of the phase diagram (see Figure 3). However, the framework of thermodynamics gives quite stringent constraints in this region. Thermodynamic stability theory gives a set of equality constraints that should be satisfied at the spinodals, as well as a set of inequality constraints that should be satisfied between the vapor and liquid spinodals. These constraints should be utilized in the future development of multiparameter EoS, both to find the appropriate functional form as well as the feasible values of the fitting parameters. A single-component fluid becomes mechanically unstable at both the vapor spinodal ($\rho = \rho_s^g$) and the liquid spinodal ($\rho = \rho_s^l$):[62]

$$(\partial P/\partial V)_{T,N} = 0 \tag{7}$$

and remains mechanically unstable between the two spinodals ($\rho_s^g < \rho < \rho_s^l$):[62]

$$(\partial P/\partial V)_{T,N} > 0 \tag{8}$$

where $N$ is the total number of particles and $V$ is the total volume. Moreover, after partial integration, the equilibrium conditions and the Gibbs−Duhem equation give the following integral:

$$\int_{\rho_{eq}^g}^{\rho_{eq}^l} (P(\rho) - P_{eq})\frac{1}{\rho^2}\,d\rho = 0 \tag{9}$$

where the last eq 9, which further constrains the behavior of the fluid in the unstable domain is automatically taken care of if saturation data are used in the fitting routine. The above equations are by no means exhaustive in constraining the thermodynamic properties of the homogeneous fluid in the unstable region. A comprehensive discussion of such constraints is given in ref 63. Such constraints and the requirement of continuity of many thermodynamic variables and their derivatives at $\rho_s^g$ and $\rho_s^l$, constrain the thermodynamic state to such an extent, that if the thermodynamic state of the fluid is determined to a reasonable accuracy up to the spinodals, the properties of the homogeneous fluid in the unstable region will also be determined to a good accuracy because of the constraints.

**Challenges with Second-Derivative Properties and the Critical Region for the SAFT Family.** Having a single Maxwell loop in the two-phase region is only one out of many constraints that physical considerations and theory impose on an EoS. Aside from the challenge with the second artificial Maxwell loop, multiparameter EoS generally describe the physical behavior of fluids well, even when extrapolated to extreme conditions. For instance, at low temperatures the virial coefficients approach negative infinity, and at high temperatures and densities the isotherms do not cross each other.[28] However, although any modeling approach that derives the thermodynamic properties from a single fundamental relation (e.g., the Helmholtz energy) is usually called "consistent", there is in fact no EoS today that satisfies all qualitative constraints imposed from theory. For example, they may have incorrect scaling behavior in vicinity of the spinodal and the vapor−liquid critical point, or crossing isotherms at high temperatures.

In addition to exhibiting incorrect critical scaling behavior, some of the more modern EoS also fail to reproduce the pure-component critical temperature and pressure. This includes most association EoS, e.g. CPA and SAFT. Association EoS explicitly account for hydrogen bonding between molecules through an additive contribution to the system's Helmholtz energy, called the Wertheim contribution.[64−67] The currently most popular SAFT models are variants of PC-SAFT[21,22] and CPA.[33] The pure-component parameters in these models are usually fitted to vapor pressures and liquid volumes along the saturation line, a practice that usually makes them overestimate the critical temperature $T_c$ and pressure $P_c$. These models can be perilous to use in applications in which the operating region contains the critical point. Figure 7 plots the phase envelope of

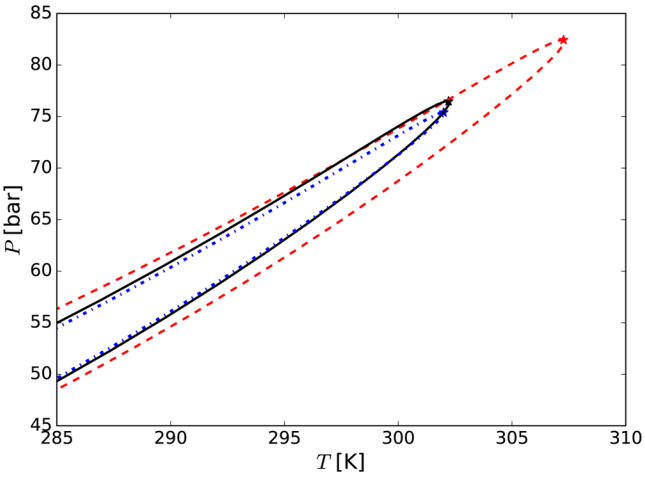


**Figure 7.** Phase envelope of a mixture of 97 mol % $CO_2$ and 3 mol % $CH_4$, computed from PC-SAFT (red dashed lines), SRK (blue dash-dot lines), and EOS-CG (black solid lines), with the critical points marked with stars. Parameters for PC-SAFT are taken from ref 21.

a $CO_2$-rich mixture with a very small amount of methane, and illustrates how the problems manifest themselves for mixtures. The most accurate EoS available for this particular mixture is EoS-CG, which is a multiparameter EoS recently developed for combustion gases.[68] While the cubic EoS SRK predicts a phase envelope (blue dash−dot lines) and a critical point of the mixture which is very close to those from EoS-CG (solid lines), PC-SAFT gives a significantly different phase-envelope (red dashed lines).

Since most EoS are so-called mean field theories they have mean field critical exponents and cannot be fitted to reproduce the critical region behavior.[69,70] It may therefore be sensible to exclude the critical region when fitting pure-component parameters to saturation data, for example by only using data


DOI: 10.1021/acs.iecr.7b00317
Ind. Eng. Chem. Res. 2017, 56, 3503−3515

at temperatures $T < 0.95T_c$. To accurately model the critical region, one needs multiparameter EoS with special terms tailor-made for the critical region, or mean-field theories coupled with so-called crossover approaches.[27] However, we do point out that it is often possible to "build in" the correct pure-component critical temperature and pressure into the model, like for cubic EoS. For example, by introducing an additional pure-component parameter, Polishuk developed a version of PC-SAFT[71] that reproduces $(T_c, P_c)$ exactly for nonassociating components.

A common problem for many EoS, including cubic EoS, CPA, and most SAFT approaches, is the poor correlation of isochoric heat capacity and speed of sound.[72] However, by replacing the traditional square-well interaction potential in the underlying theory with the more sophisticated Mie potential (a generalized Lennard-Jones potential), Lafitte et al.[73] have been able to greatly remedy these problems with their SAFT-VR Mie equation of state. This equation of state also exists in a group contribution version called SAFT-$\gamma$ Mie.[23]

**Developing Extended Corresponding State EoS for Simultaneous Speed and Accuracy for Mixtures.** For computationally demanding research challenges, in for example, computational fluid dynamics or process simulations, computationally efficient EoS are needed. At present, the most popular choice for this purpose is the cubic EoS. Unfortunately, cubic EoS are in general inaccurate for predicting properties such as the density and the speed of sound in the liquid phase (although the density predictions can be partially remedied through "volume shifts"[30]). According to Andreko,[74] cubic EoS have reached their full maturity, at least for the typical mixture of nonpolar components. The representation of volumetric properties has been improved within the limits imposed by the cubic form by extending them to as much as five parameters.[74] There is thus a need for EoS that are more accurate, but only give a moderate increase in computational time. Extended corresponding state EoS are promising candidates for this purpose.

Corresponding state principles are well-known and thoroughly described, for instance in ref 75. The basis for the theory comes from dimensional analysis of the configurational portion of the statistical mechanical partition function that leads to expressions for residual thermodynamic properties as dimensionless groups. Originally it was developed as a simple two-parameter principle, which expressed the residual compressibility factor as a function of the reduced temperature and the reduced molar volume, and thus required only the critical temperature and density for the reference fluid and the real fluid in order to estimate the thermodynamic properties. Experiments have shown that this is a good approximation for heavy noble gases and for approximately spherical molecules such as oxygen and methane. For other fluids, the corresponding state principle needs to be extended.

In the "extended corresponding state" methodology, more parameters are used in the description of the fluid. Pitzer's acentric factor, $\omega$, is well-known as a third parameter and is used, for instance by Lee and Kesler in their EoS.[76] Alternatively, the simple two-parameter corresponding state principle can be extended by making the intermolecular potential a function of the thermodynamic state and some additional characterization parameter. This makes calculation of the dimensionless volume and temperature more complicated through the introduction of shape factors:

$$\hat{V} = \frac{V}{V_c\phi(T, \omega)}, \qquad \hat{T} = \frac{T}{T_c\theta(T, \omega)} \tag{10}$$

Equations of state that use the shape factors, $\phi$ and $\theta$, are referred to as extended corresponding state EoS. In the original two-parameter corresponding state principle, both shape factors are equal to 1. The extended corresponding state methodology is associated with three main choices:

- choice of reference fluid
- choice of reference EoS
- choice of methodology to compute the shape factors

A computationally efficient variant of the extended corresponding state methodology is to employ an accurate multiparameter equation of state to describe the reference fluid and a cubic EoS to compute the shape factors. This has been referred to by Michelsen and Mollerup as "the ultimate two-parameter EoS".[25] Following previous work on this topic, we shall refer to this methodology as the SPUNG EoS.[31]

Next, we shall compare the computational efficiency and accuracy of the SPUNG methodology to the performance of the cubic EoS SRK,[11] and the multiparameter EoS for natural gas mixtures, GERG-2008.[20] We examine two versions of the SPUNG EoS, which both use SRK to compute the shape factors and propane as reference fluid, but employ different EoS for the reference fluid. The first investigated variant of SPUNG is SPUNG-MBW which uses the mBWR EoS for propane presented in 1987 by Younglove and Ely[78] as reference EoS. The second variant of SPUNG is SPUNG-MUL which uses the state-of-the-art multiparameter EoS for propane presented in 2009 by Lemmon et al.[28] as reference EoS.

**Speed Test.** To examine the computational efficiency of the SPUNG methodology, we measured the CPU time (best of three runs) for phase equilibrium calculations with various mixtures with the temperature and pressure as variables. The mixtures consisted of two to six of the main species in natural gas. The phase equilibrium calculations were performed on an equispaced 100 × 100 grid in $(T, P)$ space in the range 230−500 K and 1−300 bar. Table 1 reports the CPU time of the EoS relative to the CPU time of SRK. The computational speed of SPUNG-MBW is very similar to that of SPUNG-MUL, so we have only reported the results from SPUNG-MUL in the table. The table shows that while the SPUNG methodology only uses about twice the CPU time of SRK, the CPU time of GERG-2008 is one to two orders of magnitude larger. While the CPU time of the SPUNG methodology relative to SRK remains constant as a function of the number of components in the mixture, the relative CPU time of GERG-2008 increases linearly with a factor of ∼60. Therefore, multiparameter EoS become very computationally demanding for applications with a large number of components, such as in process simulations.

**Table 1. CPU Time Relative to SRK for Mixtures with an Increasing Number of Components**[a]

| | no. of components | | | | |
|---|---|---|---|---|---|
| EoS | 2 | 3 | 4 | 5 | 6 |
| SPUNG-MUL | 2.0 | 1.7 | 2.0 | 2.2 | 2.1 |
| GERG-2008 | 38.9 | 92.6 | 151.4 | 195.6 | 275.9 |

[a]The components in the following list were added sequentially: methane, carbon dioxide, nitrogen, ethane, propane, and *n*-butane.



DOI: 10.1021/acs.iecr.7b00317
Ind. Eng. Chem. Res. 2017, 56, 3503−3515

Table 2. Pure-Component Percentage Deviation from to GERG-2008 in the Single-Phase Regions[a]

| | molar volume | | | heat capacity | | | speed of sound | | |
|---|---|---|---|---|---|---|---|---|---|
| | | | | Methane | | | | | |
| EoS | liq | vap | sup | liq | vap | sup | liq | vap | sup |
| SRK | 3.3 | 0.2 | 1.2 | 8.9 | 3.4 | 1.6 | 13.5 | 0.3 | 2.0 |
| SPUNG-MBW | 4.3 | 0.2 | 1.0 | 3.9 | 1.6 | 0.5 | 7.9 | 0.3 | 0.9 |
| SPUNG-MUL | 4.3 | 0.2 | 1.0 | 3.7 | 0.9 | 0.2 | 7.6 | 0.2 | 1.0 |
| | | | | Carbon Dioxide | | | | | |
| SRK | 11.2 | 0.5 | 2.8 | 7.8 | 6.5 | 1.7 | 14.8 | 0.9 | 3.9 |
| SPUNG-MBW | 1.5 | 0.05 | 0.7 | 2.6 | 1.0 | 0.6 | 7.1 | 0.2 | 1.3 |
| SPUNG-MUL | 1.5 | 0.1 | 0.7 | 3.1 | 0.7 | 0.4 | 6.2 | 0.1 | 1.1 |

[a]Notation: liquid, liq; vapor, vap; supercritical, sup.

*Single-Phase Pure-Component Accuracy Tests.* We next tested the accuracy of the SPUNG methodology. Since GERG-2008 represents most of the available experimental data within their uncertainty,[20] it was used as reference. The percentage deviation in Table 2 has thus been calculated relative to GERG-2008. We have chosen 1000 points from the liquid, vapor, and supercritical regions, respectively. The liquid and vapor ranges span from the triple point temperature to $T_c$ and from 0.01 bar to 1.5 $P_c$, while the supercritical domain has been defined to be in the range $1.05T_c$–$2T_c$, $0.5P_c$– $2P_c$, where $T_c$ and $P_c$ are respectively the critical temperature and pressure. Table 2 reports the accuracy of SRK and the SPUNG variants relative to GERG-2008 for methane and carbon dioxide.

Table 2 contains the percentage deviation relative to GERG-2008 for the molar volume, the heat capacity, and the speed of sound in the liquid phase, the vapor phase, and the supercritical region. Except for the liquid phase density of methane, the SPUNG methodology displays a significantly better accuracy than SRK, in particular in the liquid and supercritical regions. The table shows that the deviation between GERG-2008 and the SPUNG methodology is insensitive to the choice of reference EoS, since the accuracy of SPUNG-MBW is very similar to the accuracy of SPUNG-MUL.

*Two-Phase Accuracy Tests.* The binary system methane/carbon dioxide is one of the few binary systems for which a "binary specific departure function" was developed for GERG-2008, meaning that its properties are especially well-fitted. We therefore sampled five vapor–liquid equilibrium (VLE) concentrations from each of the five equispaced isotherms between 230 to 300 K. We next fitted binary interaction parameters for SRK and the two versions of SPUNG to these data. This resulted in interaction parameters with the values 0.11548, 0.11551, and 0.11374 for SRK, SPUNG-MBW, and SPUNG-MUL, respectively. The investigated EoS displayed a similar accuracy for the prediction of liquid-phase compositions with an absolute average deviation (AAD) of around 8%. The EoS SRK predicted the vapor-phase concentrations more accurately than SPUNG with an AAD of 3%. In comparison, both variants of the SPUNG methodology predicted the vapor-phase VLE concentrations with an AAD of ∼11%. Figure 8 shows clearly that SRK (solid lines) follows GERG-2008 (bullets) more closely than SPUNG (dashed and dotted lines). The deviations are largest around the cricondenbar, not far from the critical point. Since SPUNG-MBW and SPUNG-MUL display very similar accuracy in Table 2 and exhibit the same deviations in VLE-predictions as shown in Figure 8, the present drawbacks of the SPUNG methodology cannot be attributed to the reference EoS. Thus, further development of extended corresponding state EoS should focus on refining the methodology for calculating the shape factors, in particular in the vicinity of the critical point.

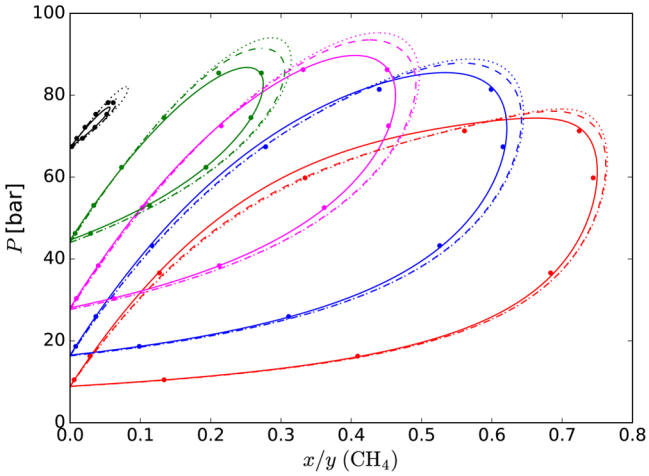


**Figure 8.** VLE predictions for $CH_4$–$CO_2$ by SRK (solid lines), SPUNG-MBW (dashed line), and SPUNG-MUL (dotted lines), in comparison to GERG-2008 (bullets). The five phase envelopes are at equidistant temperatures in the range 230–300 K.

**Developing Thermodynamic Models in Combination with Phase and Reaction Equilibria.** Routines for robust and time-efficient phase-equilibrium calculations represent one of the most important components of a modern thermodynamic framework.[25] For many applications, EoS and phase-equilibrium calculations can be treated as decoupled parts, since algorithms for phase equilibrium calculations are readily available.[25]

For mixtures such as $CO_2$–$H_2O$–$H_2S$, the phase equilibrium is established simultaneously as reactions occur in the liquid phase, where hydrosulfuric acid, carbonic acid, and other species may form. To develop predictive thermodynamic models for such complicated fluid mixtures, it is necessary to develop EoS in close combination with phase and reaction equilibria as illustrated in Figure 2.

The water chemistry of acid gases such as $CO_2$ and $H_2S$ cannot be fully described by considering only binary interactions and phase equilibrium calculations, such as in the treatment by multiparameter EoS, association models, and activity coefficient models. This is because the $CO_2$ dissociation in water affects the $H_2S$ dissociation. Nonetheless, acid gases are usually described without considering chemical reactions. Venkatraman et al.[79] described to some extent the ternary $CO_2$–$H_2S$–$H_2S$ system at 393 K. However, other acids and a shift in pH will interfere with the system, requiring a


DOI: 10.1021/acs.iecr.7b00317
Ind. Eng. Chem. Res. 2017, 56, 3503–3515

description of the chemical equilibrium to obtain a predictive model.

For some binary mixtures, such as $CO_2$−$H_2O$, it is possible to model the system to a good accuracy without considering reactions, even though carbonic acid, bicarbonate, and carbonate are reaction products.[81] For other binary systems such as $NH_3$−$CO_2$, in which the molecules in the gas phase react to form urea and water,[80] it is necessary to employ phase- and reaction-equilibrium theory for an accurate representation of the system. Figure 9 illustrates how the bubble points

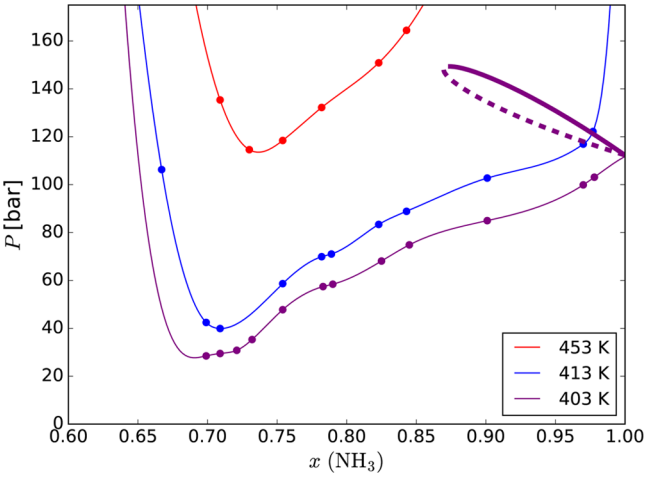


**Figure 9.** Bubble point measurements (dots) of the $NH_3$−$CO_2$ system[80] at different temperatures (colors). The curves through the dots are splines used for illustration. The thick purple curves are bubble point (solid) and dew point (dashed) predictions from PC-SAFT at 403 K.

predicted by PC-SAFT at 403 K (thick purple curve) follow a different trend than the experimental data (thin purple curve). Changing the association scheme or using a different value of the binary interaction parameter will not solve this problem, as these modifications fail to accommodate for the reactions that occur in the system. Other EoS such as cubic EoS are also incapable of reproducing the experimental trends, and give two-phase envelopes qualitatively similar to those predicted by PC-SAFT (not shown).

Other examples where reaction and phase equilibria occur simultaneously are molecules that form dimers, such as nitric oxide (NO)[82] and acetic acid ($CH_3CO_2H$).[83] The topic of reactive distillation involves both phase equilibrium and chemical reactions.[84,85] To have a predictive thermodynamic framework for fluids with simultaneous reaction and phase equilibria is clearly beneficial in this context.

For a given temperature and pressure, the phase equilibrium represents a global minimum of the Gibbs free energy. The inclusion of chemical reactions introduces constrains to the minimization problem due to the conservation of elements. Chemical reactions are typically treated using a stoichiometric or a nonstoichiometric approach.[86] The stoichiometric approach defines a set of independent stoichiometric equations, and relates mole numbers to the extent of these reactions. The nonstoichiometric approach treats the constraints in terms of Lagrange multipliers, giving more variables than the stoichiometric approach.

The Brinkley−NASA−RAND (BNR) approaches are based on the nonstoichiometric formulation.[86] The RAND method[87] was initially developed for ideal solutions, but was later extended to nonideal systems.[88] The extended RAND method converges quadratically, and automatically satisfies the element balances equations in every iteration, making this a popular method.

During the solution of the isothermal−isobaric flash problem, the number of phases is not known in advance, and must be determined. For phase equilibrium calculations, this is most commonly accomplished by using tangent plane analysis.[77,89] In this endeavor, it is a large advantage to have thermodynamically consistent EoS with only one Maxwell loop in the two-phase region.

For equilibrium between reactive phases, the tangent plane becomes constrained,[90] and a condition similar to the tangent plane has been developed from the Karush−Kuhn−Tucker optimality condition of the reactive flash system.[91,92] McKinnon and Mongeau[93] later developed a generic global optimization algorithm for the chemical and phase equilibrium problem applying the constrained tangent plane.

Michelsen states that the modified phase stability criterion can be applied to chemically reacting systems,[77] and several works have relied on tangent plane analysis for phase stability.[94−97] The early work on ideal solutions by Gautam and Seider[98] also uses a similar approach, where a limited number of phases are defined initially and new phases are included if required. Jalali et al.[99] use methods from applied mathematics, homotopy continuation, as a global method solving the combined phase and chemical reaction equilibrium problem. Wasylkiewicz[100] base their reactive flash algorithm on variable transformation and location of all stationary points of the tangent plane distance function.

The review article of Seider and Widagdo[101] discusses some aspects of phase stability for reactive multiphase systems, but it is apparent that there is less consensus on how to solve this problem optimally, and that several approaches are capable of predicting phase and chemical reaction equilibria in multiphase systems.

Efficient methods for calculation of critical points in nonreactive systems were established in the early eighties.[102,103] However, in systems with reaction and phase equilibrium, the mixture composition is no longer constant and the problem becomes increasingly more difficult. Using the variable transformation for reactive systems introduced by Ung and Doherty,[104] the critical condition of Heidemann and Khalil[102] can be solved for reactive systems.[105,106] Nevertheless, numerically efficient plotting of phase envelopes and calculation of critical points in reactive systems remain research topics under development.

To devise predictive models for mixtures such as $CO_2$−$H_2O$−$H_2S$, the thermodynamic model must be developed in close connection with reactive phase equilibria. From the previous discussion, it is clear that further work to develop robust and reliable algorithms for this purpose is needed.

## ■ CONCLUSION

In this work, we have discussed the present challenges associated with the modern thermodynamic modeling framework, focusing on the model-specific routines (equations of state) and the model-independent routines (phase and chemical equilibrium calculations). We have discussed how the accuracy, computational efficiency, and predictive ability of the current thermodynamic framework can be improved.



DOI: 10.1021/acs.iecr.7b00317
Ind. Eng. Chem. Res. 2017, 56, 3503−3515

The most accurate equations of state (EoS) available today, multiparameter EoS, have a second artificial Maxwell loop in the two-phase region that is responsible for many of their present shortcomings. We elaborated how thermodynamically consistent multiparameter EoS with a single Maxwell loop can be developed by exploiting superstabilization and hybrid data sets in the metastable regions and appropriate constraints in the unstable region of the phase diagram for the single-component homogeneous fluid. Multiparameter EoS with a single Maxwell loop hold the potential to significantly increase the accuracy of mass-based density functional theory for description of equilibrium and nonequilibrium interfacial phenomena.

Sufficiently far away from the critical point, the molecular-based SAFT family of EoS are often the best choice when predictive ability is important, for example, for systems with strongly associating fluids or polymers for which few experimental data are available. However, this type of EoS is currently unable to match the experimental critical point of associating fluids. A research challenge is thus to improve the prediction of the critical point, which would enable more accurate representation of vapor−liquid equilibria, in particular for mixtures.

To combine a thermodynamic framework with computationally demanding process simulations or computational fluid dynamics requires computationally efficient EoS. We showed that an extended corresponding state EoS where a cubic equation of state was used to calculate the shape factors and a multiparameter equation of state was used as reference fluid gave significantly more accurate predictions of the density, the heat capacity, and the speed of sound in the liquid and the supercritical phases than cubic EoS, with a mere doubling of the computational time. In comparison, the computational time of multiparameter EoS was orders of magnitude larger. The cubic equation of state was more accurate than the extended corresponding state methodology for the prediction of vapor−liquid equilibria, and further development of the extended corresponding state methodology should focus on improving the calculation of the shape factors, in particular for mixtures in the vicinity of the critical point.

To develop predictive models for mixtures such as $CO_2$−$NH_3$ and $CO_2$−$H_2O$−$H_2S$, we elaborated how EoS must be developed in close connection with reactive phase equilibria. Further development of robust and reliable algorithms for this purpose is needed.

If current challenges associated with the modern thermodynamic frameworks are overcome, a next generation thermodynamic framework holds the potential to improve the accuracy and predictive ability in a wide range of applications such as process optimization, computational fluid dynamics, treatment of interfacial phenomena, and processes with reactive mixtures.

## AUTHOR INFORMATION


### Corresponding Author

*E-mail: oivind.wilhelmsen@ntnu.no.

### ORCID

Øivind Wilhelmsen: 0000-0003-4631-0349


### Notes

The authors declare no competing financial interest.

## ACKNOWLEDGMENTS

We thank Dr. Eric W. Lemmon for very useful discussions, and we thank Dr. Svend T. Munkejord for carefully reading through the manuscript and providing helpful comments and suggestions for improvements. The authors acknowledge support from the HYVA project.

## REFERENCES


(1) Aursand, P.; Hammer, M.; Munkejord, S. T.; Wilhelmsen, Ø. Pipeline transport of $CO_2$ mixtures: Models for transient simulation. *Int. J. Greenhouse Gas Control* **2013**, *15*, 174−185.

(2) Wilhelmsen, Ø.; Skaugen, G.; Hammer, M.; Wahl, P. E.; Morud, J. C. Time efficient solution of phase equilibria in dynamic and distributed systems with differential algebraic equation solvers. *Ind. Eng. Chem. Res.* **2013**, *52*, 2130−2140.

(3) Skaugen, G.; Kolsaker, K.; Taxt Walnum, H.; Wilhelmsen, Ø. A flexible and robust modelling framework for multi-stream heat exchangers. *Comput. Chem. Eng.* **2013**, *49*, 95−104.

(4) Skaugen, G.; Hammer, M.; Wahl, P. E.; Wilhelmsen, Ø. Constrained non-linear optimization of a process for liquefaction of natural gas including a geometrical and thermo-hydraulic model of a compact heat exchanger. *Comput. Chem. Eng.* **2015**, *73*, 102−115.

(5) Buffett, B. A. The thermal state of Earth's core. *Science* **2003**, *299*, 1675.

(6) El Mekki Azouzi, M.; Ramboz, C.; Lenain, J. F.; Caupin, F. A coherent picture of water at extreme negative pressure. *Nat. Phys.* **2013**, *9*, 38−41.

(7) Valtz, A.; Chapoy, A.; Coquelet, C.; Paricaud, P.; D, R. Vapour-liquid equilibria in the carbon dioxide-water system, measurement and modelling from 278.2 to 318.2 K. *Fluid Phase Equilib.* **2004**, *226*, 333−344.

(8) Sloan, E. D.; Koh, C. J. *Clathrate Hydrates of Natural Gases*, 3rd ed.; CRC Press: Boca Raton, 2007.

(9) Hendriks, E. M.; Kontogeorgis, G. M.; Dohrn, R.; de Hemptinne, J.-C.; Economou, I. G.; Žilnik, L. F.; Vesovic, V. Industrial Requirements for Thermodynamics and Transport Properties. *Ind. Eng. Chem. Res.* **2010**, *49*, 11131−11141.

(10) Peng, D. Y.; Robinson, D. B. A new two-constant equation of state. *Ind. Eng. Chem. Fundam.* **1976**, *15*, 59−64.

(11) Soave, G. Equilibrium constants from a Modified Redlich−Kwong Equation of State. *Chem. Eng. Sci.* **1972**, *27*, 1197−1203.

(12) Jørstad, O. *Equation of State for Hydrocarbon Mixtures*. Ph.D. Thesis, NTH-University in Trondheim, 1993.

(13) Setzmann, U.; Wagner, W. A new equation of state and tables of thermodynamic properties for methane covering the range from the melting Line to 625 K at pressures up to 1000 MPa. *J. Phys. Chem. Ref. Data* **1991**, *20*, 1061−1155.

(14) Span, R.; Wagner, W. A new equation of state for carbon dioxide covering the fluid region from the triple-point temperature to 1100 K at Pressures up to 800 MPa. *J. Phys. Chem. Ref. Data* **1996**, *25*, 1509−1596.

(15) Span, R.; Lemmon, E. W.; Jacobsen, R. T.; Wagner, W. A reference quality equation of state for nitrogen. *Int. J. Thermophys.* **1998**, *19*, 1121−1132.

(16) Tegeler, C.; Span, R.; Wagner, W. A new equation of state for argon covering the fluid region for temperatures from the melting line to 700 K at pressures up to 1000 MPa. *J. Phys. Chem. Ref. Data* **1999**, *28*, 779−850.

(17) Smukala, J.; Span, R.; Wagner, W. New equation of state for ethylene covering the fluid region for temperatures from the melting line to 450 K at pressures up to 300 MPa. *J. Phys. Chem. Ref. Data* **2000**, *29*, 1053−1121.

(18) Wagner, W.; Pruß, A. The IAPWS formulation 1995 for the thermodynamic properties of ordinary water substance for general and scientific use. *J. Phys. Chem. Ref. Data* **2002**, *31*, 387−535.

(19) Li, H.; Jakobsen, J. P.; Wilhelmsen, Ø.; Yan, J. PVTxy properties of $CO_2$ mixtures relevant for $CO_2$ capture, transport and storage: Review of available experimental data and theoretical models. *Appl. Energy* **2011**, *88*, 3567−3579.




DOI: 10.1021/acs.iecr.7b00317
*Ind. Eng. Chem. Res.* 2017, 56, 3503−3515

(20) Kunz, O.; Wagner, W. The GERG-2008 wide-range equation of state for natural gases and other mixtures: An expansion of GERG-2004. *J. Chem. Eng. Data* **2012**, *57*, 3032−3091.
(21) Gross, J.; Sadowski, G. Perturbed-Chain SAFT: An Equation of State Based on a Perturbation Theory for Chain Molecules. *Ind. Eng. Chem. Res.* **2001**, *40*, 1244−1260.
(22) Gross, J.; Sadowski, G. Application of the Perturbed-Chain SAFT Equation of State to Associating Systems. *Ind. Eng. Chem. Res.* **2002**, *41*, 5510−5515.
(23) Papaioannou, V.; Lafitte, T.; Avendaño, C.; Adjiman, C. S.; Jackson, G.; Müller, E. A.; Galindo, A. Group contribution methodology based on the statistical associating fluid theory for heteronuclear molecules formed from Mie segments. *J. Chem. Phys.* **2014**, *140*, 054107.
(24) Maribo-Mogensen, B. *Development of an electrolyte CPA equation of state for applications in the petroleum and chemical industries*. Ph.D. Thesis, Technical University of Denmark, 2014.
(25) Michelsen, M. L.; Mollerup, J. M. *Thermodynamic models: Fundamentals & computational aspects*, 2nd ed.; Tie-Line Publications: Holte, 2007.
(26) Burger, J.; Papaioannou, V.; Gopinath, S.; Jackson, G.; Galindo, A.; Adjiman, C. S. A Hierarchical Method to Integrated Solvent and Process Design of Physical $CO_2$ Absorption Using the SAFT-$\gamma$ Mie Approach. *AIChE J.* **2015**, *69*, 3249.
(27) Span, R. *Multiparameter Equations of State*; Springer-Verlag: Berlin, 2000.
(28) Lemmon, E. W.; McLinden, M. O.; Wagner, W. Thermodynamic properties of propane. III. A reference equation of state for temperatures from the melting line to 650 K and pressures up to 1000 MPa. *J. Chem. Eng. Data* **2009**, *54*, 3141−3180.
(29) Pini, M.; Spinelli, A.; Persico, G.; Rebay, S. Consistent look-up table interpolation method for real-gas flow simulations. *Comput. Fluids* **2015**, *107*, 178−188.
(30) Péneloux, A.; Rauzy, E.; Fréze, R. A consistent correction for Redlich−Kwong−Soave volumes. *Fluid Phase Equilib.* **1982**, *8*, 7−23.
(31) Wilhelmsen, Ø.; Skaugen, G.; Jørstad, O.; Li, H. Evaluation of SPUNG and other equations of atate for use in carbon capture and storage modelling. *Energy Procedia* **2012**, *23*, 236−245.
(32) Gernert, J.; Jäger, A.; Span, R. Calculation of phase equilibria for multi-component mixtures using highly accurate Helmholtz energy equations of state. *Fluid Phase Equilib.* **2014**, *375*, 209−218.
(33) Kontogeorgis, G. M.; Voutsas, E. C.; Yakoumis, I. V.; Tassios, D. P. An Equation of State for Associating Fluids. *Ind. Eng. Chem. Res.* **1996**, *35*, 4310−4318.
(34) Queimada, A. J.; Miqueu, C.; Marrucho, I. M.; Kontogeorgis, G. M.; Coutinho, J. A. P. Modeling vapor-liquid interfaces with the gradient theory in combination with the CPA equation of state. *Fluid Phase Equilib.* **2005**, *228*, 479−485.
(35) Lemmon, E. W.; Jacobsen, R. T. A new functional form and new fitting techniques for equations of state with application to pentafluoroethane (HFC-125). *J. Phys. Chem. Ref. Data* **2005**, *34*, 69−108.
(36) Elhassan, A. E.; Craven, R. J. B.; de Reuck, K. M. The Area method for pure fluids and an analysis of the two-phase region. *Fluid Phase Equilib.* **1997**, *130*, 167−187.
(37) Thol, M.; Lemmon, E. W. Equation of state for the thermodynamic properties of trans-1,3,3,3-tetrafluoropropene [R-1234ze(E)]. *Int. J. Thermophys.* **2016**, *37*, 28.
(38) Wilhelmsen, Ø.; Trinh, T. T.; Kjelstrup, S.; Bedeaux, D. Influence of curvature on the transfer coefficients for evaporation and condensation of Lennard−Jones fluid from square-gradient theory and nonequilibrium molecular dynamics. *J. Phys. Chem. C* **2015**, *119*, 8160−8173.
(39) Rowlinson, J. S. Translation of J. D. van der Waals "The thermodynamic theory of capillarity under the hypothesis of a continuous variation of density. *J. Stat. Phys.* **1979**, *20*, 197−200.
(40) Wilhelmsen, Ø.; Bedeaux, D.; Kjelstrup, S.; Reguera, D. Thermodynamic stability of nanoscale bubbles/droplets: The square gradient theory and the capillary approach. *J. Chem. Phys.* **2014**, *140*, 024704.
(41) Johnson, J. K.; Zollweg, J. A.; Gubbins, K. E. The Lennard−Jones equation of state revisited. *Mol. Phys.* **1993**, *78*, 591−618.
(42) Wilhelmsen, Ø.; Bedeaux, D.; Reguera, D. Tolman length and rigidity constants of the Lennard−Jones fluid. *J. Chem. Phys.* **2015**, *142*, 064706.
(43) van Giessen, A. E.; Blokhuis, E. M. Direct determination of the Tolman length from the bulk pressures of liquid drops via molecular dynamics simulations. *J. Chem. Phys.* **2009**, *131*, 164705.
(44) Blokhuis, E. M.; van Giessen, A. E. Density functional theory of a curved liquid-capour interface: Evaluation of the rigidity constants. *J. Phys.: Condens. Matter* **2013**, *25*, 225003.
(45) Tzotzi, C.; Bontozoglou, B.; Andritsos, N.; Vlachogiannis, M. Effect of fluid properties on flow Patterns in two-phase gas-liquid flow in horizontal and downward pipes. *Ind. Eng. Chem. Res.* **2011**, *50*, 645−655.
(46) Cornelisse, P. *Gradient Theory Applied—Simultaneous Modelling of Interfacial Tension and Phase Behaviour*. Ph.D. Thesis, Delft University of Technology, 1997.
(47) Lin, H.; Duan, Y.-Y.; Min, Q. Gradient theory modelling of surface tension for pure fluids and binary mixtures. *Fluid Phase Equilib.* **2007**, *254*, 75−90.
(48) Magnanelli, E.; Wilhelmsen, Ø.; Bedeaux, D.; Kjelstrup, S. Extending the nonequilibrium square-gradient model with temperature-dependent influence parameters. *Phys. Rev. E* **2014**, *90*, 032402.
(49) Wilhelmsen, Ø.; Bedeaux, D.; Reguera, D. Communication: Tolman length and rigidity constants of water and their role in nucleation. *J. Chem. Phys.* **2015**, *142*, 171103.
(50) Wilhelmsen, Ø.; Trinh, T. T.; Kjelstrup, S.; van Erp, T. S.; Bedeaux, D. Heat and mass transfer across interfaces in complex nanogeometries. *Phys. Rev. Lett.* **2015**, *114*, 065901.
(51) Kvamme, B.; Graue, A.; Aspenes, E.; Kuznetsova, T.; Gránásy, L.; Tóth, G.; Pusztai, T.; Tegze, G. Kinetics of solid hydrate formation by carbon dioxide: Phase field theory of hydrate nucleation and magnetic resonance imaging. *Phys. Chem. Chem. Phys.* **2004**, *6*, 2327−2334.
(52) Gránásy, L.; Pusztai, T.; Börzsönyi, T.; Warren, J. A.; Douglas, J. F. A general mechanism of polycrystalline growth. *Nat. Mater.* **2004**, *3*, 645−650.
(53) Biben, T.; Kassner, K.; Misbah, C. Phase-field approach to three-dimensional vesicle dynamics. *Phys. Rev. E* **2005**, *72*, 041921.
(54) Debenedetti, P. G.; Stanley, H. E. Supercooled and Glassy Water. *Phys. Today* **2003**, *56*, 40−46.
(55) Holten, V.; Sengers, J. V.; Anisimov, M. A. Equation of State for Supercooled Water at Pressures up to 400 MPa. *J. Phys. Chem. Ref. Data* **2014**, *43*, 043101.
(56) Wilhelmsen, Ø.; Bedeaux, D.; Kjelstrup, S.; Reguera, D. Communication: Superstabilization of fluids in nanocontainer. *J. Chem. Phys.* **2014**, *141*, 071103.
(57) Alvarenga, A. D.; Grimsditch, M.; Bodnar, R. J. Elastic properties of water under negative pressures. *J. Chem. Phys.* **1993**, *98*, 8392−8396.
(58) Potoff, J. J.; Siepmann, J. I. Vapor-liquid equilibria of mixtures containing alkanes, carbon dioxide, and nitrogen. *AIChE J.* **2001**, *47*, 1676.
(59) Wheatley, R. J.; Harvey, A. H. Intermolecular potential energy surface and second virial coefficients for the water-$CO_2$ dimer. *J. Chem. Phys.* **2011**, *134*, 134309.
(60) Meyer, C.; Harvey, A. Dew-point measurements for water in compressed carbon dioxide. *AIChE J.* **2015**, *61*, 2913−2925.
(61) Rutkai, G.; Thol, M.; Lustig, R.; Span, R.; Vrabec, J. Communication: Fundamental equation of state correlation with hybrid data sets. *J. Chem. Phys.* **2013**, *139*, 041102.
(62) Tester, J. W.; Modell, M. *Thermodynamics and its applications*; Prentice Hall: NJ, 1996.
(63) Aursand, P.; Gjennestad, M. Aa.; Aursand, E.; Hammer, M.; Wilhelmsen, Ø. The spinodal of single- and multi-component fluids


DOI: 10.1021/acs.iecr.7b00317
*Ind. Eng. Chem. Res.* 2017, 56, 3503−3515

and its role in the development of modern equations of state. *Fluid Phase Equilib.* **2016**, *436*, 98.
(64) Wertheim, M. S. Fluids with highly directional attractive forces. I. Statistical thermodynamics. *J. Stat. Phys.* **1984**, *35*, 19−34.
(65) Wertheim, M. S. Fluids with highly directional attractive forces. II. Thermodynamic perturbation theory and integral equations. *J. Stat. Phys.* **1984**, *35*, 35−47.
(66) Wertheim, M. S. Fluids with highly directional attractive forces. III. Multiple attraction sites. *J. Stat. Phys.* **1986**, *42*, 459−476.
(67) Wertheim, M. S. Fluids with highly directional attractive forces. IV. Equilibrium polymerization. *J. Stat. Phys.* **1986**, *42*, 477−492.
(68) Gernert, G.; Span, R. EOS-CCG: A Helmholtz energy mixture model for humid gases and CCS mixtures. *J. Chem. Thermodyn.* **2016**, *93*, 274−293.
(69) Fisher, M. E. The theory of equilibrium critical phenomena. *Rep. Prog. Phys.* **1967**, *30*, 615−730.
(70) Debenedetti, P. G. *Metastable Liquids: Concepts and Principles*; Princeton University Press: Princeton, 1996.
(71) Polishuk, I. Standardized Critial Point-Based Numerical Solution of Statistical Association Fluid Theory Parameters: The Perturbed Chain-Statistical Association Fluid Theory Equation of State Revisited. *Ind. Eng. Chem. Res.* **2014**, *53*, 14127−14141.
(72) De Villiers, A. J.; Schwarz, C. E.; Burger, A. J.; Kontogeorgis, G. M. Evaluation of the PC-SAFT, SAFT and CPA equations of state in predicting derivative properties of selected non-polar and hydrogen-bonding compounds. *Fluid Phase Equilib.* **2013**, *338*, 1−15.
(73) Lafitte, T.; Apostolakou, A.; Avendaño, C.; Galindo, A.; Adjiman, C. S.; Müller, E. A.; Jackson, G. Accurate statistical associating fluid theory for chain molecules formed from Mie segments. *J. Chem. Phys.* **2013**, *139*, 154504.
(74) Andreko, A. *Equations of State for Fluid Mixtures*; Sengers, J. V., Kayser, R. F., Peters, C. J., White, H. J., Eds.; IUPAC, 2000; Chapter Cubic and Generalized van der Waals Equations, pp 76−119.
(75) Ely, J. F.; Marrucho, I. M. F. In *Equations of State for Fluid Mixtures*; Sengers, J. V., Kayser, R. F., Peters, C. J, White, H. J, Eds.; IUPAC, 2000; Chapter The Corresponding-states Principle, pp 289−320.
(76) Lee, B. I.; Kesler, M. G. A Generalized Thermodynamic Correlation Based on Three-Parameter Corresponding States. *AIChE J.* **1975**, *21*, 510−527.
(77) Michelsen, M. L. The isothermal flash problem. Part I. Stability analysis. *Fluid Phase Equilib.* **1982**, *9*, 1−19.
(78) Younglove, B. A.; Ely, J. F. Thermophysical Properties of Fluids. II. Methane, Ethane, Propane, Isobutane, and Normal Butane. *J. Phys. Chem. Ref. Data* **1987**, *16*, 577−798.
(79) Venkatraman, A.; Lake, L. W.; Johns, R. T. Gibbs Free Energy Minimization for Prediction of Solubility of Acid Gases in Water. *Ind. Eng. Chem. Res.* **2014**, *53*, 6157−6168.
(80) Lemkowitz, S.; Goedegebuur, J.; Berg, P. Bubble point measurements in the ammonia-carbon dioxide system. *J. Appl. Chem. Biotechnol.* **1971**, *21*, 229−232.
(81) Aasen, A.; Hammer, M.; Skaugen, G.; Jakobsen, J.; Wilhelmsen, Ø. Thermodynamic models to accurately describe the *PVTxy*-behavior of water/carbon dioxide mixtures. *Fluid Phase Equilib.* **2017**, DOI: 10.1016/j.fluid.2017.02.006. Accepted for publication.
(82) Lachet, V.; Creton, B.; de Bruin, T.; Bourasseau, E.; Desbiens, N.; Wilhelmsen, Ø.; Hammer, M. Equilibrium and transport properties of $CO_2$ + $N_2O$ and $CO_2$+NO mixtures: Molecular simulation and equation of state modelling study. *Fluid Phase Equilib.* **2012**, *322*, 66−78.
(83) Briggs, J. M.; Nguyen, T. B.; Jorgensen, W. L. Monte Carlo simulations of liquid acetic acid and methyl acetate with the OPLS potential functions. *J. Phys. Chem.* **1991**, *95*, 3315−3322.
(84) Ung, S.; Doherty, M. F. Vapor-liquid phase equilibrium in systems with multiple chemical reactions. *Chem. Eng. Sci.* **1995**, *50*, 23−48.
(85) Avami, A.; Saboohi, Y. A simultaneous method for phase identification and equilibrium calculations in reactive mixtures. *Chem. Eng. Res. Des.* **2011**, *89*, 1901−1908.
(86) Smith, W. R.; Missen, R. W. *Chemical Reaction Equilibrium Analysis: Theory and Algorithms*; Wiley-Interscience: New York, USA, 1982.
(87) White, W. B.; Johnson, S. M.; Dantzig, G. B. Chemical Equilibrium in Complex Mixtures. *J. Chem. Phys.* **1958**, *28*, 751−755.
(88) Greiner, H. An efficient implementation of Newton's method for complex nonideal chemical equilibria. *Comput. Chem. Eng.* **1991**, *15*, 115−123.
(89) Baker, L. E.; Pierce, A. C.; Luks, K. D. Gibbs Energy Analysis of Phase Equilibria. *SPEJ, Soc. Pet. Eng. J.* **1982**, *22*, 738−742.
(90) Smith, J. V.; Missen, R. W.; Smith, W. R. General optimality criteria for multiphase multireaction chemical equilibrium. *AIChE J.* **1993**, *39*, 707−710.
(91) Jiang, Y.; Smith, W. R.; Chapman, G. R. Global Optimality Conditions and their Geometric Interpretation for the Chemical and Phase Equilibrium Problem. *SIAM J. Optimiz.* **1995**, *5*, 813−834.
(92) Jiang, Y.; Chapman, G.; Smith, W. On the geometry of chemical reaction and phase equilibria. *Fluid Phase Equilib.* **1996**, *118*, 77−102.
(93) McKinnon, K.; Mongeau, M. A Generic Global Optimization Algorithm for the Chemical and Phase Equilibrium Problem. *J. Global Optim.* **1998**, *12*, 325−351.
(94) Castier, M.; Rasmussen, P.; Fredenslund, A. Calculation of simultaneous chemical and phase equilibria in nonideal systems. *Chem. Eng. Sci.* **1989**, *44*, 237−248.
(95) Gupta, A. K.; Bishnoi, P. R.; Kalogerakis, N. A method for the simultaneous phase equilibria and stability calculations for multiphase reacting and non-reacting systems. *Fluid Phase Equilib.* **1991**, *63*, 65−89.
(96) Pérez Cisneros, E. S.; Gani, R.; Michelsen, M. Reactive separation systems−I. Computation of physical and chemical equilibrium. *Chem. Eng. Sci.* **1997**, *52*, 527−543.
(97) Phoenix, A. V.; Heidemann, R. A. A non-ideal multiphase chemical equilibrium algorithm. *Fluid Phase Equilib.* **1998**, *150−151*, 255−265.
(98) Gautam, R.; Seider, W. D. Computation of phase and chemical equilibrium: Part II. Phase-splitting. *AIChE J.* **1979**, *25*, 999−1006.
(99) Jalali, F.; Seader, J.; Khaleghi, S. Global solution approaches in equilibrium and stability analysis using homotopy continuation in the complex domain. *Comput. Chem. Eng.* **2008**, *32*, 2333−2345.
(100) Wasylkiewicz, S. K. Transformed molar Gibbs free energy of mixing in multireaction systems. *Chem. Eng. Sci.* **2000**, *55*, 5177−5182.
(101) Seider, W. D.; Widagdo, S. Multiphase equilibria of reactive systems. *Fluid Phase Equilib.* **1996**, *123*, 283−303.
(102) Heidemann, R. A.; Khalil, A. M. The calculation of critical points. *AIChE J.* **1980**, *26*, 769−779.
(103) Michelsen, M. L. Calculation of critical points and phase boundaries in the critical region. *Fluid Phase Equilib.* **1984**, *16*, 57−76.
(104) Ung, S.; Doherty, M. F. Theory of phase equilibria in multireaction systems. *Chem. Eng. Sci.* **1995**, *50*, 3201−3216.
(105) Platt, G. M.; Medeiros, J. L. d. Phase rule calculations and the thermodynamics of reactive systems under chemical equilibrium. *Braz. J. Chem. Eng.* **1999**, *16*, 247−265.
(106) Sanchéz-Mares, F.; Bonilla-Petriciolet, A.; Segovia-Hernández, J. G.; Tapia-Picazo, J. C.; Ponsich, A. *Calculation of Critical Points in Reactive Mixtures Using a Global Optimization Approach*. 18th European Symposium on Computer Aided Process Engineering—ESCAPE 18, 2008.


DOI: 10.1021/acs.iecr.7b00317
*Ind. Eng. Chem. Res.* 2017, 56, 3503−3515